Controlling the Outcome of Electron Transfer Reactions in Ionic Liquids

Harsha V. R. Annapureddy and Claudio J. Margulis*

Department of Chemistry, The University of Iowa, Iowa City, Iowa 52242

Received: June 1, 2009; Revised Manuscript Received: July 10, 2009

In this article, we investigate the excited state intramolecular electron transfer (ET) reaction of crystal violet lactone (CVL) in the room temperature ionic liquid (RTIL) *N*-propyl-*N*-methylpyrrolidinium bis(trifluoromethylsulfonyl)imide $[Pr_{31}^+][Tf_2N^-]$. This system was chosen in light of recent experimental observations by Maroncelli and co-workers (*J. Phys. Chem. B* **2007**, *111*, 13473), in which the kinetics of electron transfer between S_1 (commonly referred as LE) and S_2 (commonly referred as CT) emission states and, therefore, the ratio of emitting populations were shown to be absorption-wavelength-dependent. Our computational studies indicate that the kinetics of the intramolecular ET between S_1 and S_2 states of CVL in $[Pr_{31}^+][Tf_2N^-]$ is local solvent-environment-dependent. Because emission time scales are smaller than solvent relaxation time scales, this behavior is characteristic of RTILs but uncommon in conventional solvents. Therefore, RTILs open a window of opportunity for manipulating the outcome of chemical reactions simply by tunning the initial excitation wavelength. Our studies show that when acetonitrile is used as a solvent instead of $[Pr_{31}^+][Tf_2N^-]$ the ratio of populations of emission states is independent of excitation wavelength, eliminating the opportunity for influencing the outcome of reactions.

1. Introduction

Ionic liquids (ILs) have been branded tailor-made compounds because of the large number of combinations of ions that can be used to generate them. The truth is that they are more of a designer nightmare. One has almost infinite flexibility in choosing cations and anions, but little is known about what the exact properties of the new liquids will turn out to be once they are made.

Although being able to predict bulk IL properties such as densities and viscosities is very important, it is also in the finer details, in the difference in molecular time scales and length scales across ILs that key issues related to chemical outcome control linger and make ILs truly designer materials.

Ionic liquids are different from most other materials because they provide the designer with at least one extra control variable. One can design or choose to work with liquids with specific relaxation time scales. These relaxation time scales control the speed for transitioning between the dynamically heterogeneous regime and the normal homogeneous liquid regime. In different ILs at room temperature, this happens on a range of time scales from 100 ps to 100 ns.

Several recent studies[1−18] have proven that reactants are often distributed in environments that can be experimentally identified and selected.[1−9,19] These selected environments are in slow exchange.

The ability for spatial selection is not unique to ILs; for example, one can do a hole burning experiment in any liquid. Instead, it is the time scale during which these environments remain almost unchanged that is unique to ILs and useful. Our main assertion is that in ILs, selection of solvent environments is equivalent to chemical reactivity control. This option for control is absent in liquids in which the solvent responds fast, as compared to the time scale for transition state formation in ground state reactions or excited state lifetimes in excited state chemistry. It is in this sense that RTILs present us with a totally new solvation paradigm. On a macroscopic time scale, ILs are normal, homogeneous liquids; on a microscopic time scale, they are not.

As has been previously shown,[20−25] Marcus theory can be applied in ILs. In a set of very interesting articles, Lynden-Bell and co-workers[20−23] as well as Kim and co-workers[24,25] have demonstrated that reaction free energies for electron transfer processes in ILs are Marcus-like in that their functional form is quadratic. As we will show in subsequent sections, we also find this to be true. Local environments may favor different products both because barriers to interconversion (and therefore, rate constants) are locally different and also because free energy differences (and therefore, thermodynamic constants) are also locally different. This leads to ranges of local free energy differences and local rate constants.

Different ILs display these characteristics to different extents. A deep understanding of the dynamics in different RTILs will determine our ability to better control the outcome of chemical reactions. Obviously, the opportunity for chemical control is not restricted to photoactivated processes. Selectivity could possibly be achieved, for example, by controlling an electrochemical potential.

Samanta and co-workers[26−29] found that under certain circumstances, the fluorescence response of probes in RTILs can be dependent on the excitation wavelength, a phenomenon known as red-edge effect. This phenomenon is observable only when excited state lifetimes are short when compared with solvent relaxation time scales. Using the same concept, recently, Maroncelli and co-workers[8] explored the excitation wavelength dependence of electron transfer between two polar excited states of crystal violet lactone (CVL) in IL *N*-propyl-*N*-methylpyrrolidinium bis(trifluoromethylsulfonyl)imide ($[Pr_{31}^+][Tf_2N^-]$) (see Figures 1 and 2). CVL is a dual fluorescent molecule. Extensive studies by Karpiuk[30] had previously shown that the photoexcitation of CVL into the S_1 state with dipole moment of 11D is localized on the aminophthalide ring. Subsequent electron

* To whom correspondence should be addressed. E-mail: claudio-margulis@uiowa.edu.

10.1021/jp905144n CCC: $40.75
Published on Web 08/10/2009

transfer from one of the dimethylaniline groups to the aminophthalide group results in the formation of the more polar S_2 state with a dipole moment of 25D. The emission spectra of CVL in different polar solvents show two peaks corresponding to electronic decay from S_1 and S_2, respectively. Maroncelli and co-workers found that upon photoexcitation of CVL in $[Pr_{31}^+][Tf_2N^-]$ at different wavelengths, the emission intensities of these two peaks varied significantly.

This dependence of the electron transfer product distribution on the excitation wavelength is absent in normal solvents.

2. Methods

We performed molecular dynamics (MD) simulation for the CVL in the $[Pr_{31}^+][Tf_2N^-]$ system recently studied by Jin and co-workers.[8] For comparison, we also performed MD simulations of CVL in acetonitrile. All simulations were carried out using the AMBER 9 package.[31]

All trajectories in the RTIL consisted of a single flexible CVL molecule solvated by 150 $[Pr_{31}^+][Tf_2N^-]$ ion pairs. Simulations in acetonitrile consisted of a single CVL molecule solvated by 424 acetonitrile molecules.

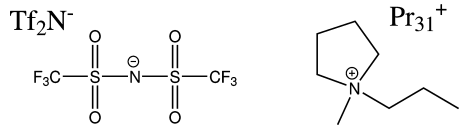

Figure 1. *N*-Propyl-*N*-methylpyrrolidinium bis(trifluoromethylsulfonyl)imide ($[Pr_{31}^+][Tf_2N^-]$).

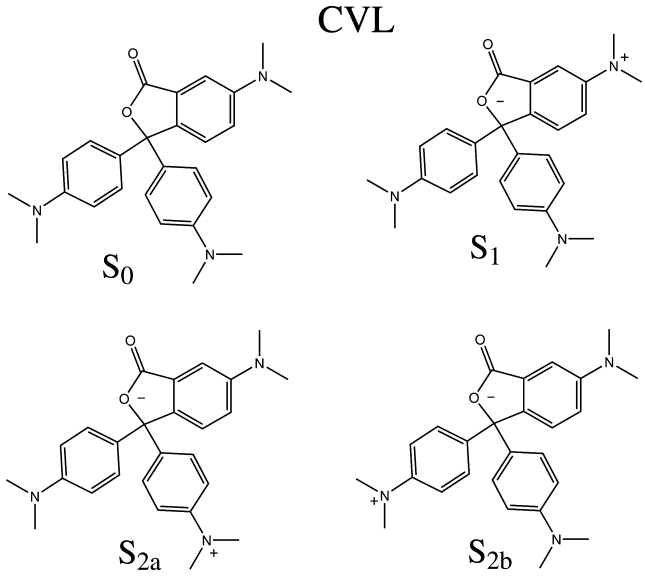

Figure 2. Fluorescent probe: crystal violet lactone (CVL).

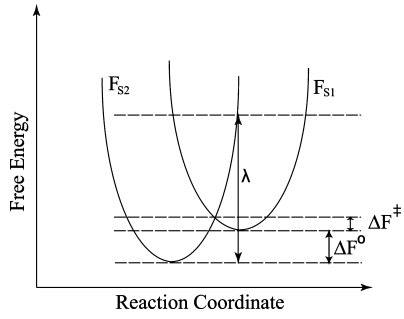

Figure 3. Cartoon defining various quantities of the Marcus parabolas.

All systems were thoroughly equilibrated for several nanoseconds. Ionic liquids are particularly notorious for the difficulty in obtaining truly equilibrated initial conditions. To make sure the systems were correctly equilibrated, we lowered and raised the total charge of the ions, and we also performed runs at high temperature and later slowly annealed the system to match experimental conditions. These equilibration runs were performed in the NPT (constant number of particles, pressure, and temperature) ensemble using the Berendsen algorithm. Final simulation box sizes were 40.5 Å in the case of the RTIL and 34.3 Å in the case of acetonitrile.

Once systems were properly equilibrated at 300 K, NVE (constant number of particles, volume, and energy) production runs were launched using the same methodology as in refs 10−13.

Specifically, to compute emission spectra, we first run an ensemble of equilibrated trajectories in the ground electronic state for one nanosecond and then simulate instantaneous vertical excitation by changing potential parameters to those of states S_1 and S_2. In the case of the free energy calculations, we wait for 700 ps after photoexcitation for short time-scale transients to dissapear and then collect data from each trajectory for a period of 1.3 ns.

We used the "Leap-frog" integration algorithm implemented in AMBER 9 for all our simulations. Cutoffs for both the Lennard-Jones and Coulombic interactions were set to 10 Å. To deal with long-range electrostatic interactions, the PME algorithm was used. Identical schemes were used in simulations of CVL in acetonitrile.

Potential energy parameters for the $[Tf_2N^-]$ anion are taken from the work of Lopes and Pádua,[32] whereas for the $[Pr_{31}^+]$ cation, charges are those in reference 33, and all other parameters are taken from the generalized AMBER force field.[31]

Except for the charges, all parameters for CVL in the ground and excited states are taken to be identical and obtained from the generalized AMBER force field.[31] In all cases, interactions are taken as in the AMBER force field convention in which intramolecular nonbonded energies are neglected for atoms that are less than three bonds apart and are reduced to 50% for the atoms separated exactly by three bonds. Parameters for acetonitrile are taken from the literature 34.

Ground-state charges for CVL were obtained from an ab initio ESP-fit at the Hartree−Fock (HF)/6-31G* theory level using the Gaussian program[35] and are reported as Supporting Information.

Generating a model for the excited states of CVL is complex. Electronically excited state calculations for this molecule yield a large number of states with similar energies and dipole moments. Our task was greatly facilitated by a very insightful article by Karpiuk[30] in which he demonstrates that the two states involved in electron transfer are localized. Specifically, the S_1 excitation is localized on the aminophthalide ring, and emission from this state is almost identical to that of fragment 6-dimethylaminophtalide, a much simpler molecule. A highly accurate CASSCF electronic structure calculation for the S_1 state of 6-dimethylaminophtalide is available in the literature.[36] Minor modifications to the differences in partial charges between ground and excited states reported for 6-dimethylaminophtalide generate a model for the S_1 state of CVL with the correct dipole moment (11D).

By studying malachite green lactone, which is also a fragment of CVL, Karpiuk demonstrated that the electron transfer to generate S_2 comes from one of the dimethylaniline groups. In the gas phase, since these two dimethylaniline groups are

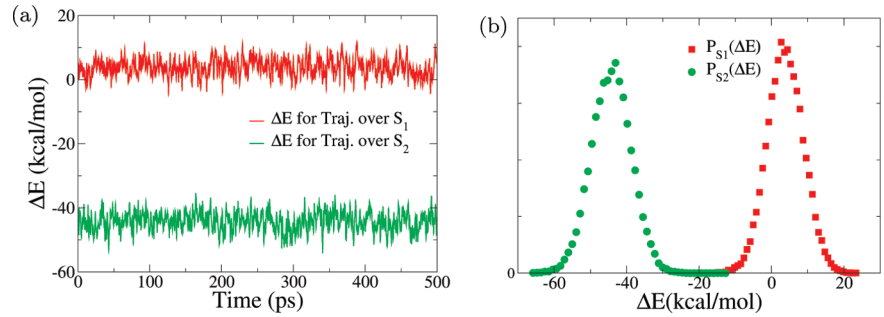

Figure 4. (a) ΔE (red) for trajectory in electronic state S_1 and (green) for trajectory in electronic state S_2. (b) Probability distribution functions $P_{S_1}(\Delta E)$ and $P_{S_2}(\Delta E)$.

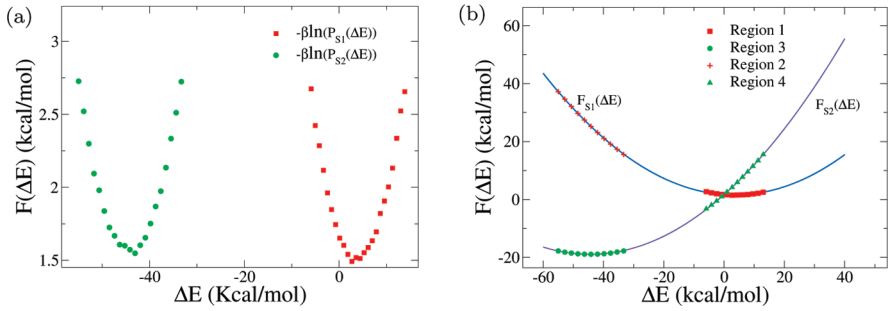

Figure 5. (a) $-kt \times \ln(P_{S_1}(\Delta E))$ and $-kt \times \ln(P_{S_2}(\Delta E))$. (b) Free energy curves obtained from simulation and by extrapolation as described in the text.

symmetrical, either of them can act as the electron donor. In a liquid, the situation is different, and the surrounding solvent will impose a bias. To model the two local diabatic states S_{2a} and S_{2b} shown in Figure 2 that give rise to adiabatic state S_2, we use an empirical valence bond (EVB) approach.[37,38] The charges for the diabatic representations of S_2 are obtained by applying the changes in partial charges obtained for S_1 at the location of the amino group in the aminophthalide fragment to the amino group of either dimethylaniline fragments. Small adjustments were made to match the dipole moment of S_2 (25D). All charges for the ground and excited state models of CVL are reported as Supporting Information.

The reactive S_2 potential is defined over the lowest adiabatic surface obtained by diagonalization of the EVB Hamiltonian matrix in eq 1.

$$\mathbf{H} = \begin{bmatrix} H_{11} & H_{12} \\ H_{21} & H_{22} \end{bmatrix} \tag{1}$$

In eq 1, the matrix elements H_{11} and H_{22} are the diabatic energies of states S_{2a} and S_{2b} depicted in Figure 2. Since the S_2 state is recognized to be highly localized, the coupling element H_{12} and H_{21} are assumed to be small. In our simulations, these weak coupling elements were taken to be constant at a value of 1.0 kcal/mol.

As will be shown, although these models are not prefect, they are able to qualitatively capture the correct changes in energetics as polarity changes from that in the gas phase to that in polar solvents. A detailed description of our methodology for computing the absorption-wavelength-dependent emission spectra of the probe in ionic liquids can be found in previous publications.[12,13,39] The emission energy ΔE_{em} from S_1 to S_0 or from S_2 to S_0 can be expressed as in eq 2.

$$\Delta E_{em} = \Delta E(g) + \Delta E_{sol} \tag{2}$$

Here, $\Delta E(g)$ denotes the gas-phase or intramolecular energy difference that is independent of the solvent. This value cannot be obtained from classical molecular dynamics simulations but is experimentally accessible and can be found in the literature both for the S_1-to-S_0 (27 180 cm^{-1}) and S_2-to-S_0 (30 165 cm^{-1}) transitions.[30]

ΔE_{sol} is the solute−solvent interaction energy difference arising from the distinct charge distributions in the ground and excited electronic states.

In the gas phase, $\Delta E_{em} = \Delta E(g)$ and $\Delta\Delta E = \Delta E_{emS_2} - \Delta E_{emS_1} = 2985\ cm^{-1}$. Interestingly, in a polar solvent, the value of $\Delta\Delta E$ becomes negative. As an example, judging from Figure 3 in reference 30, in acetonitrile, $\Delta\Delta E$ obtained as the difference in the frequencies between the maximum of emission of S_2 and S_1 is approximately $-$ 6500 cm^{-1}. Our parametrization of the excited state potentials in the presence of acetonitrile yields a value of $\Delta\Delta E = -9000 cm^{-1}$, which although not perfect, correctly captures the change in sign and, correspondingly, the change in energy ordering of the two excited states.

$$I_{ab}(\Delta E_{ex}) = \sum_l I^l_{ab}(\Delta E_{ex}) \tag{3}$$

$$I^l_{em}(\Delta E_{em}) = \int_0^\infty \delta(\Delta E(t) - \Delta E_{em}) \times e^{-t/\tau_f}\, dt \tag{4}$$

$$I_{em}(\Delta E_{ex}, \Delta E_{em}) = \sum_l I^l_{em}(\Delta E_{em})\, I^l_{ab}(\Delta E_{ex}) \tag{5}$$

Excitation-frequency-dependent emission intensities are computed using eqs 3−5, as in refs 12, 13, and 39. Here, $I^l_{ab}(\Delta E_{ex})$ is the probability distribution of absorption energy gaps, ΔE_{ex}, in trajectory l. $I_{ab}(\Delta E_{ex})$ denotes the total probability distribution at vertical transition excitation energy ΔE_{ex} computed as a sum over all trajectories. $I^l_{em}(\Delta E_{em})$ is the corresponding steady-state probability distribution of emission energy gaps ΔE_{em} weighted

by an exponential decay corresponding to the lifetime (τ_f) of the probe (here assumed to be 1 ns) for trajectory l. $I_{em}(\Delta E_{ex}, \Delta E_{em})$ denotes the intensity or joint probability distribution of emission energy ΔE_{em} when excitation energy is ΔE_{ex}. In the calculation of $I_{em}(\Delta E_{ex}, \Delta E_{em})$, ΔE_{ex} is to state S_1. All spectra are reported as area-normalized.

In the canonical ensemble, the Helmholtz free energy, F, is

$$F = -RT \times \ln(Q) \tag{6}$$

where Q is the canonical partition function. The free energy as a function of a special coordinate is

$$\begin{aligned} F(x) &= -kT \times \ln(Q(x)) \\ &= -kT \times \ln\left(\int d\bar{r} e^{-\beta E(x,\bar{r})}\right) \\ &= -kT \times \ln\left(\frac{\int d\bar{r} e^{-\beta E(x,\bar{r})}}{\int dx\, d\bar{r} e^{-\beta E(x,\bar{r})}} \times \int dx\, d\bar{r} e^{-\beta E(x,\bar{r})}\right) \\ &= -kT \times \ln(P(x)) - kT \times \ln(Q) \\ &= -kT \times \ln(P(x)) + F \end{aligned} \tag{7}$$

where $P(x)$ is the probability distribution function for coordinate x.

Defining $F_{S_1}(x)$ and $F_{S_2}(x)$ as the corresponding free energy functions in two different electronic states, S_1 and S_2, one has

$$\begin{aligned} F_{S_1}(x) - F_{S_2}(x) &= (F_{S_1} - F_{S_2}) - kT \times \ln\left(\frac{P_{S_1}(x)}{P_{S_2}(x)}\right) \\ &= F_{S_1} - F_{S_2} - kT \times \\ &\quad \ln\left(\frac{\int d\bar{r} e^{-\beta E_{S_1}(x,\bar{r})}}{\int d\bar{r} e^{-\beta E_{S_2}(x,\bar{r})}} \times \frac{\int dx\, d\bar{r} e^{-\beta E_{S_2}(x,\bar{r})}}{\int dx\, d\bar{r} e^{-\beta E_{S_1}(x,\bar{r})}}\right) \\ &= -kT \times \ln\left(\frac{\int d\bar{r} e^{-\beta E_{S_1}(x,\bar{r})}}{\int d\bar{r} e^{-\beta E_{S_2}(x,\bar{r})}}\right) \end{aligned} \tag{8}$$

If, as in previous publications,[40−44] the order parameter x used as a reaction coordinate for the calculation of free energies is defined as

$$x = \Delta E = E_{S_2} - E_{S_1} \tag{9}$$

then $E_{S_2} = E_{S_1} + x$ and

$$\begin{aligned} F_{S_1}(x) - F_{S_2}(x) &= -kT \times \ln\left(\frac{\int d\bar{r} e^{-\beta E_{S_1}(x,\bar{r})}}{\int d\bar{r} e^{-\beta x} e^{-\beta E_{S_1}(x,\bar{r})}}\right) \\ &= -x \end{aligned} \tag{10}$$

then

$$\Delta F(\Delta E) = F_{S_2}(\Delta E) - F_{S_1}(\Delta E) = \Delta E \tag{11}$$

If Marcus theory is applicable, then the two free energy curves should be parabolas of identical curvature (see Figure 3). A combination of eqs 8 and 11 with the Marcus assumption is sufficient to algebraically define the curvature of $F_{S_1}(\Delta E)$ and $F_{S_2}(\Delta E)$ as well as the value of the Helmholtz free energy difference $\Delta F^0 = F_{S_2} - F_{S_1}$.

$$\begin{aligned} \Delta E &= \Delta F^0 - kT \times \ln\left(P_{S_2}(\Delta E)\right) + kT \times \ln\left(P_{S_1}(\Delta E)\right) \\ &= \Delta F^0 + \gamma(\Delta E - \Delta E_{S_2})^2 - \gamma(\Delta E - \Delta E_{S_1})^2 \end{aligned}$$

which leads to the set of equations

$$\Delta F^0 = \gamma\left(\Delta E_{S_1}{}^2 - \Delta E_{S_2}{}^2\right) \tag{12}$$

$$\Delta E_{S_1} - \Delta E_{S_2} = \frac{1}{2\gamma} \tag{13}$$

Here, ΔE_{S_1} and ΔE_{S_2} are the corresponding average values of the energy gap, $E_{S_2} - E_{S_1}$, over two trajectories with identical initial conditions but with dynamics driven by states S_1 and state S_2, respectively, such as shown in Figure 4a, for which statistics is always very good. Since only two numbers, namely, ΔE_{S_1} and ΔE_{S_2}, are needed to establish the curvature of the free energies and ΔF^0, one can use the rest of the data to verify whether the Marcus approximation is valid. Using an approach similar to that described by Tachiya,[42] eq 11 can be used to extrapolate the free energy to regions that are not sampled during simulations. As an example, using data from two trajectories—one run with potential corresponding to state S_1, and the other corresponding to state S_2, ΔE can be computed. With these data, probability distribution functions and $-kT \ln(P(\Delta E))$ can be computed as in Figures 4b and 5a. For each electronic state, the functions displayed in Figure 5a sample only regions around equilibrium.

Using eq 11 and ΔF^0 as an adjustable constant, these functions can be extended without invoking the Marcus approximation. Color-coded segments in Figure 5b indicate how one can extend the Helmholtz free energy function for state S_1 by using data around the equilibrium configuration of state S_2 and vice versa. Region 1 (red ■ of S_1) is used to obtain region 4 of S_2, and region 3 (green ●) of S_2 is used to obtain region 2 of S_1.

If the overall curves $F_{S_2}(\Delta E)$ and $F_{S_1}(\Delta E)$ can be made to overlap with the Marcus parabolae computed only from the values ΔE_{S_1} and ΔE_{S_2}, then the approximation is verified.

It is important to emphasize that ΔE_{S_1} and ΔE_{S_2} energy differences, such as those shown in Figure 4a, are local in nature. By this, we mean that because of the slow nature of the solvent on a time scale relevant to the electron transfer process, ΔE_{S_1} and ΔE_{S_2} are not the same for all trajectories; instead, they are local solvent-environment-dependent.

Parallel to the way in which we compute absorption-wavelength-dependent emission spectra, one can compute the joint probability $P_{S_1}(\Delta E_{ex}, \Delta E)$ of observing during simulation an energy gap between the two excited states, $E_{S_2} - E_{S_1} = \Delta E$, given that the dynamics is driven by state S_1 when CVL was originally photoexcited into state S_1 with energy ΔE_{ex}.

$$P_{S_1}(\Delta E_{ex}, \Delta E) = \sum_l P^l_{S_1}(\Delta E)\, P^l_{ab}(\Delta E_{ex}) \tag{14}$$

$$P_{S_2}(\Delta E_{ex}, \Delta E) = \sum_l P^l_{S_2}(\Delta E)\, P^l_{ab}(\Delta E_{ex}) \qquad (15)$$

Similarly, $P_{S_2}(\Delta E_{ex}, \Delta E)$ is the joint probability distribution of ΔE with dynamics driven by S_2 when the excitation energy into S_1 is ΔE_{ex}. These two probability distributions are used to compute excitation-frequency-dependent free energy curves.

3. Results and Discussion

Figure 6 shows computed emission spectra from CVL fluorescent states S_1 and S_2 for an ensemble of trajectories in acetonitrile. Consistent with Karpiuk's[30] experiments, the fluorescence emission of state S_2 appears at lower energy. All independent NVE simulations result in almost identical spectra. Consistent with these results, free energies computed from our ensemble of independent calculations show almost identical Marcus parabolas shown in Figure 10.

The case of CVL in RTIL is quite different. If we consider the emission from S_1 and S_2 states without allowing for electron transfer, one obtains the spectra in Figure 7a (corresponding absorption spectra are provided as Supporting Information). The emission spectrum of each independent trajectory is significantly different. This is a phenomenon that we have previously explained[12,39] and that is commonly experimentally observed in ionic liquids because of heterogeneity and slow dynamics. Key experimental articles describing this type of behavior are those by Samanta and co-workers[26−29] and Sarkar and co-workers.[9,16−18]

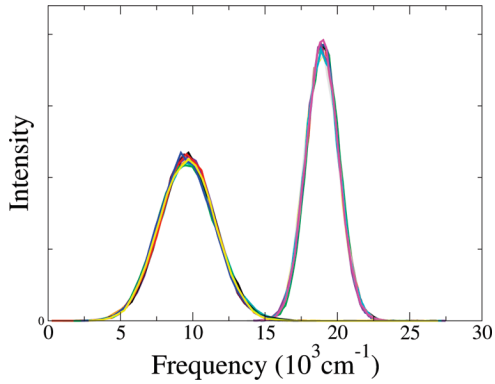

Figure 6. Emission spectra of S_1 and S_2 states of CVL in acetonitrile. The set of curves on the right correspond to emission from state S_1, and the set of curves on the left correspond to emission from state S_2. Each line corresponds to a different molecular dynamics trajectory.

Clearly, the differences in emission spectra are due to the fact that each independent trajectory has CVL in a different local environment, and these environments are in slow exchange on a time scale compatible with the lifetime of either excited states of CVL. The most interesting aspect of this observation is that this heterogeneity can be exploited by photoselecting probe molecules that are in particular solvent environments. Just like in a normal hole burning experiment, by changing the frequency of the incident light, one can selectively excite a subensemble of fluorophores, the main difference being that in the RTIL, the memory of this photoselection remains active throughout the lifetime of either excited state. In essence, these subensembles experience different surrounding local solvent polarities that are not time-averaged on a time scale of the lifetime of the excited state molecule. Of course, photoselection also occurs in acetonitrile, but memory of this is lost within the first few picoseconds of excited state life.

It is interesting to consider the special case of one of our trajectories driven by S_2, shown in dashes in Figure 7a. If we closely observe this spectrum, we see that it has two peaks, both corresponding to S_2 emission. In Figure 7b, we show ΔE_{em} as a function of time for this particular trajectory. It is clear that we are capturing a rare reorganization event, since it occurs in only one of our trajectories. The fact that these events are uncommon explains why each trajectory has a different spectrum on this time scale.

In Figure 8, we show the excitation-frequency-dependent emission spectra calculated using eq 5. We can clearly see that

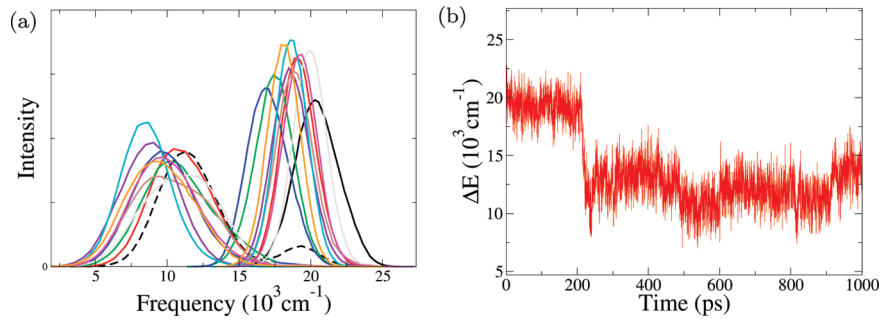

Figure 7. (a) Emission spectra of S_1 and S_2 states of CVL in $[Pr_{31}^+][Tf_2N^-]$. The set of curves on the right correspond to emission from state S_1, and the set of curves on the left correspond to emission from state S_2. Each line corresponds to a different molecular dynamics trajectory. (b) ΔE as a function of time for the trajectory giving rise to the spectrum in part a represented with dotted lines.

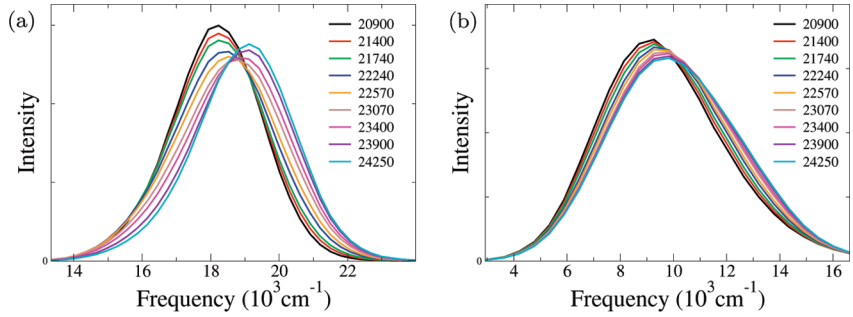

Figure 8. Excitation-dependent emission spectra (a) for S_1 and (b) for S_2. Absorption frequencies in legend are in units of cm^{-1}.

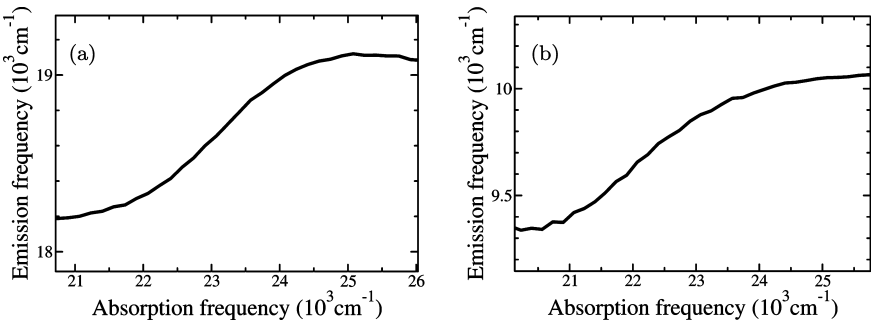

Figure 9. Peaks of emission spectrum vs the excitation frequency (a) for S_1 and (b) for S_2.

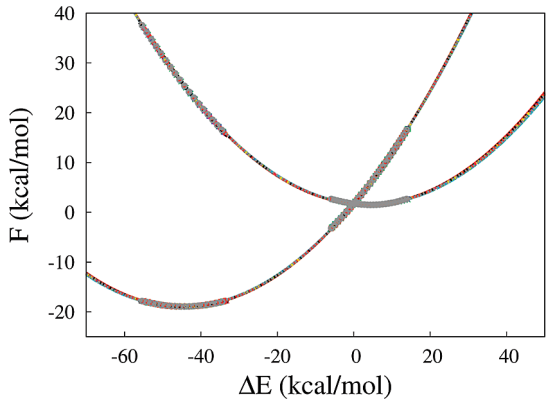

Figure 10. Free energy curves for intramolecular electron transfer of CVL in acetonitrile. The curves on the right of each graph are for F_{S_1}, and curves on the left are for F_{S_2}. Each curve with different color represents a different MD trajectory.

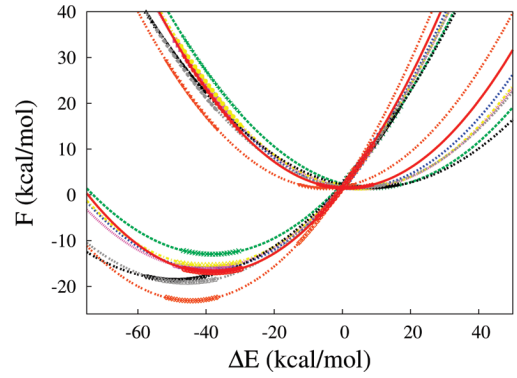

Figure 11. Free energy curves for intramolecular electron transfer of CVL in RTIL. The curves on the right of each graph are for F_{S_1}, and curves on the left are for F_{S_2}. Each curve with different color represents a different MD trajectory.

TABLE 1: Parameters Obtained by Fitting the Free Energy Data to Quadratic Equation $y = a(x - b)^2 + c^a$

	F_{S_1}			F_{S_2}		
traj	a	b	c	a	b	c
			ACN			
1	0.0104	3.48	1.54	0.0104	−44.47	−18.95
2	0.0102	3.94	1.54	0.0102	−44.92	−18.95
3	0.0103	3.73	1.54	0.0103	−44.72	−18.95
4	0.0103	3.78	1.55	0.0103	−44.80	−18.96
5	0.0102	3.97	1.56	0.0102	−44.99	−18.95
6	0.0103	3.68	1.55	0.0103	−44.70	−18.96
7	0.0104	3.59	1.55	0.0104	−44.63	−18.97
8	0.0103	3.76	1.54	0.0103	−44.74	−18.95
9	0.0103	3.86	1.56	0.0103	−44.86	−18.95
10	0.0102	4.09	1.56	0.0102	−45.12	−18.95
			IL			
1	0.0122	0.70	1.50	0.0122	−40.42	−18.37
2	0.0106	9.19	1.53	0.0106	−38.15	−12.94
3	0.0116	3.77	1.51	0.0116	−39.34	−16.27
4	0.0109	5.34	1.52	0.0109	−40.62	−16.12
5	0.0090	8.73	1.58	0.0090	−47.05	−17.59
6	0.0112	5.34	1.52	0.0112	−39.35	−15.49
7	0.0087	8.68	1.58	0.0087	−48.80	−18.48
8	0.0127	−4.91	1.49	0.0127	−44.30	−23.12
9	0.0100	4.26	1.55	0.0100	−45.62	−19.13
10	0.0127	1.25	1.48	0.0127	−38.13	−16.96

[a] x and y are in units of kcal/mol.

the emission spectra from S_1 and S_2 are red-shifted upon excitation toward the lower frequencies. In Figure 9, we also show the maximum of emission plotted against excitation energies. These results qualitatively agree with the experiments of Maroncelli and co-workers.[8] In their work, they observed a shift of 350 cm^{-1}, whereas we observe a shift of 900 cm^{-1}. Although our results are exaggerated, we are successful in capturing the correct trend.

In Figure 11, we show free energy curves for the electron transfer process between S_1 and S_2 in the ionic liquid. Interest-

TABLE 2: Solvation free energy $\Delta F°$, activation free energy $\Delta F^{‡}$, and reorganization free energy λ in kcal/mol

traj	$\Delta F^{‡}$	ΔF^{0}	λ
	ACN		
1	0.13	20.50	23.98
2	0.16	20.49	24.43
3	0.14	20.50	24.22
4	0.15	20.51	24.29
5	0.16	20.51	24.48
6	0.14	20.51	24.19
7	0.13	20.52	24.11
8	0.15	20.49	24.25
9	0.15	20.50	24.36
10	0.17	20.51	24.60
	IL		
1	0.01	19.86	20.56
2	0.89	14.48	23.67
3	0.16	17.79	21.55
4	0.31	17.64	22.98
5	0.68	19.16	27.89
6	0.32	17.00	22.34
7	0.66	20.06	28.74
8	0.31	24.61	19.70
9	0.18	20.68	24.94
10	0.02	18.44	19.69

ingly and consistent with the work of Kim and Lynden Bell,[20−25] each couple of trajectories in the same local environment but under different electronic potentials corresponding to S_1 and S_2 gives rise to color-coded free energy curves that satisfy the Marcus relationship; however, these Marcus curves are different in each local environment!

When we compare our free energy curves computed in acetonitrile with those in the ionic liquid, it is quite obvious that the kinetics and thermodynamics of electron transfer will be absorption-wavelength-dependent in the RTIL but independent in the conventional solvent. In fact, what this means is that the RTIL offers an extra degree of control on chemical reactivity. We can rationally choose to modify the outcome of an electron transfer reaction simply by means of initial subensemble selection.

If we look at the values in Table 1, we see that the curvatures of the parabolas in different local environments are different in the case of the RTIL but not in the case of acetonitrile. The curvature of the free energy is directly related to the polarity of the solvent around the solute.[44] In Table 2, we report the free energies computed from various pairs of trajectories characterized by their local environment. The definitions of the various Helmholtz free energy quantities are displayed in Figure 3. These values clearly show the difference between conventional polar solvents and this RTIL. In the case of the RTIL, the solvation free energies (ΔF^{0}) are significantly different for the various environments, but they are basically identical in the case of acetonitrile. Similarly, the activation free energies ($\Delta F^{‡}$) and, therefore, the local kinetics as well as the solvent reorganization free energies (λ) are also significantly different in the RTIL.

$$k \propto e^{-\beta \Delta F^{‡}} \tag{16}$$

According to transition state theory, the rate constant for reaction k depends on the activation energy, as in eq 16. The electron transfer process between excited states of CVL has different activation energies, so one can expect to have locally different transfer rates. Table 1 shows the value of the curvatures for F_{S_1} and F_{S_2} computed independently for each particular pair of trajectories in the same local environment. Since in each case local curvatures are almost identical for states S_1 and S_2, Marcus theory is locally applicable. However, an analysis across trajectories demonstrates that reaction kinetics at each local environment level will be significantly different.

It is important to emphasize that our classical calculations can access only the solvent contribution to the free energy. To compare with the exact experimental kinetic values obtained by Jin and co-workers,[8] we would need to account for the correct solute contribution to the free energy and for quantum factors. Nonetheless, one can use our results to test the trends to be expected if the electron transfer process occurred in the normal and inverted regions.

In Figure 12, we show our excitation-wavelength-dependent free energy curves computed using eqs 14 and 15. It is clear that as the excitation energy increases, the solvent contribution to the free energy barrier for electron transfer also increases. This is also shown in Figure 13.

In our study, the electron transfer appears to occur in the normal Marcus region. If we displace the Marcus parabolas such that they intersect in the inverted region, we see in Figure 14 that the trend in activation energies gets reversed.

In the experiments of Jin and co-workers,[8] an increase in the ratio $r = I_{S_2}/I_{S_1}$ (where I_{S_1} and I_{S_2} are the intensities of emission from S_1 and S_2, respectively) was observed with red-edge excitation. This experimental observation is consistent with the system being in the normal region.

4. Conclusions

In this work, we demonstrated that the thermodynamics and kinetics of intramolecular electron transfer following photoexcitation of CVL in $[Pr_{31}^{+}][Tf_2N^{-}]$ is local solvent-environment-dependent. Our results provide molecular level understanding of recent experiments in the Maroncelli group[8] in which intramolecular electron transfer of CVL was observed to be an absorption-wavelength-dependent process. Due to the time scale

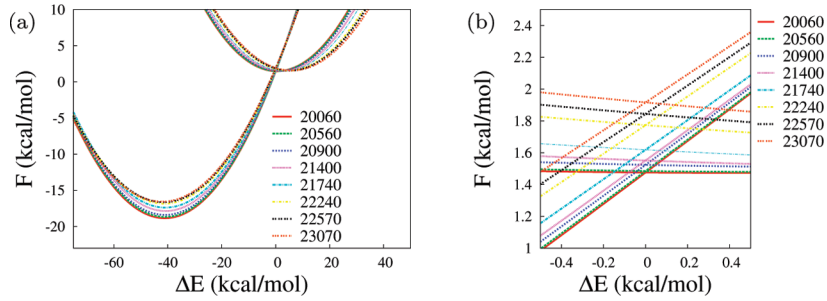

Figure 12. Free energy plots at various excitation frequencies: (a) complete curves and (b) near the crossing point. Absorption frequencies in legend are in units of cm^{-1}.

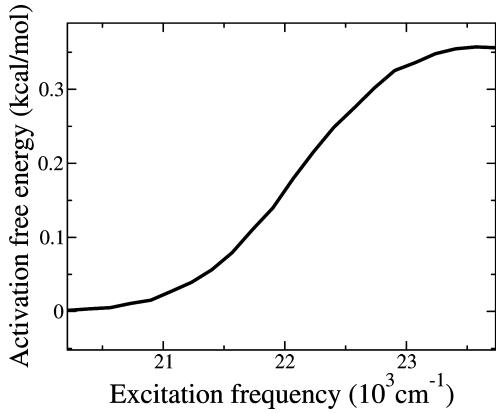

Figure 13. Activation free energy ($\Delta F^{\ddagger}$) vs excitation frequency.

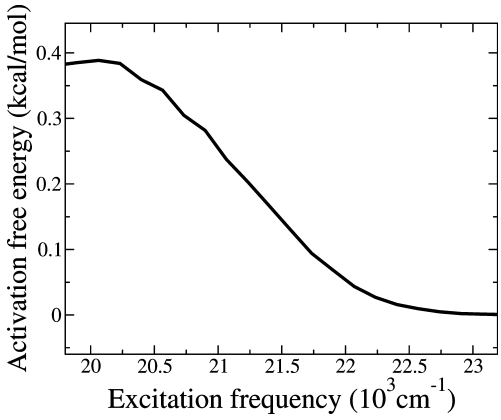

Figure 14. Activation free energy ($\Delta F^{\ddagger}$) vs excitation frequency in the inverted region.

separation between the electron transfer process (fast) and the dynamics of the solvent (slow) by selective red-edge excitation, one is able to influence the outcome of an electron transfer reaction. On the contrary, in acetonitrile, the outcome of the electron transfer reaction is independent of excitation frequency.

Acknowledgment. C.J.M. and H.V.R.A. thank Prof. Maroncelli for insightful discussions. This material is based upon work supported by the National Science Foundation under Grant CAREER#0547640 awarded to C.J.M. Any opinions, findings, and conclusions or recommendations expressed in this material are those of the author(s) and do not necessarily reflect the views of the National Science Foundation.

Supporting Information Available: Charges for the different states of CVL and corresponding trajectory-dependent absorption spectra are provided as Supporting Information. This information is available free of charge via the Internet at http://pubs.acs.org.

References and Notes

(1) Karmakar, R.; Samanta, A. *Chem. Phys. Lett.* **2003**, *376*, 638–645.
(2) Karmakar, R.; Samanta, A. *J. Phys. Chem. A* **2003**, *107*, 7340–7346.
(3) Karmakar, R.; Samanta, A. *J. Phys. Chem. A* **2002**, *106*, 4447–4452.
(4) Karmakar, R.; Samanta, A. *J. Phys. Chem. A* **2002**, *106*, 6670–6675.
(5) Arzhantsev, S.; Jin, H.; Baker, G. A.; Maroncelli, M. *J. Phys. Chem. B* **2007**, *111*, 4978–4989.
(6) Arzhantsev, S.; Jin, H.; Ito, N.; Maroncelli, M. *Chem. Phys. Lett.* **2006**, *417*, 524–529.
(7) Jin, H.; Baker, G. A.; Arzhantsev, S.; Dong, J.; Maroncelli, M. *J. Phys. Chem. B* **2007**, *111*, 7291–7302.
(8) Jin, H.; Li, X.; Maroncelli, M. *J. Phys. Chem. B* **2007**, *111*, 13473–13478.
(9) Chakrabarty, D.; Seth, D.; Chakraborty, A.; Sarkar, N. *J. Phys. Chem. B* **2005**, *109*, 5753–5758.
(10) Hu, Z.; Margulis, C. J. *Acc. Chem. Res.* **2007**, *40*, 1097–1105.
(11) Hu, Z.; Margulis, C. *J. Phys. Chem. B* **2007**, *111*, 4705–4714.
(12) Hu, Z.; Margulis, C. J. *Proc. Natl. Acad. Sci. U.S.A.* **2006**, *103*, 831–836.
(13) Annapureddy, H. V. R.; Hu, Z.; Xia, J.; Margulis, C. J. *J. Phys. Chem. B* **2008**, *112*, 1770–1776.
(14) Jiang, W.; Wang, Y.; Voth, G. A. *J. Phys. Chem. B* **2007**, *111*, 4812–4818.
(15) Wang, Y.; Voth, G. A. *J. Am. Chem. Soc.* **2005**, *127*, 12192–12193.
(16) Chakrabarty, D.; Chakraborty, A.; Seth, D.; Sarkar, N. *J. Phys. Chem. A* **2005**, *109*, 1764–1769.
(17) Chakrabarty, D.; Chakraborty, A.; Seth, D.; Hazra, P.; Sarkar, N. *Chem. Phys. Lett.* **2004**, *397*, 469–474.
(18) Chakrabarty, D.; Hazra, P.; Chakraborty, A.; Seth, D.; Sarkar, N. *Chem. Phys. Lett.* **2003**, *381*, 697–704.
(19) Del Popolo, M. G.; Voth, G. A. *J. Phys. Chem. B* **2004**, *108*, 1744–1752.
(20) Lynden-Bell, R. M. *Electrochem. Commun.* **2007**, *9*, 1857–1861.
(21) Lynden-Bell, R. M. *J. Phys. Chem. B* **2007**, *111*, 10800–10806.
(22) Lynden-Bell, R. M. *J. Chem. Phys.* **2008**, *129*, 204503.
(23) Streeter, I.; Lynden-Bell, R. M.; Compton, R. G. *J. Phys. Chem. C* **2008**, *112*, 14538–14544.
(24) Shim, Y.; Kim, H. J. *J. Phys. Chem. B* **2007**, *111*, 4510–4519.
(25) Shim, Y.; Jeong, D.; Manjari, S.; Choi, M. Y.; Kim, H. J. *Acc. Chem. Res.* **2007**, *40*, 1130–1137.
(26) Mandal, P.; Sarkar, M.; Samanta, A. *J. Phys. Chem. A* **2004**, *104*, 9048–9053.
(27) Mandal, P. K.; Paul, A.; Samanta, A. *J. Photochem. Photobiol. A* **2006**, *182*, 113–120.
(28) Paul, A.; Mandal, P. K.; Samanta, A. *J. Phys. Chem. B* **2005**, *109*, 9148–9153.
(29) Samanta, A. *J. Phys. Chem. B* **2006**, *110*, 13704–13716.
(30) Karpiuk, J. *J. Phys. Chem. A* **2004**, *108*, 11183–11195.
(31) Case, D.; Darden, T. A.; Cheatham, T. E., III; Simmerling, C. L.; Wang, J.; Duke, R. E.; Luo, R.; Merz, K. M.; Pearlman, D. A.; Crowley, M.; Walker, R. C.; Zhang, W.; Wang, B.; Hayik, S.; Roitberg, A.; Seabra, G.; Wong, K. F.; Paesani, F.; Wu, X.; Brozell, S.; Tsui, V.; Gohlke, H.; Yang, L.; Tan, C.; Mongan, J.; Hornak, V.; Cui, G.; Beroza, P.; Mathews, D. H.; Schafmeister, C.; Ross, W. S.; Kollman, P. A. *AMBER 9*; University of California, San Fransisco: San Fransisco, CA, 2006.
(32) Lopes, J. N. C.; Padua, A. A. H. *J. Phys. Chem. B* **2004**, *108*, 16893–16898.
(33) Canongia Lopes, J. N.; Padua, A. A. H. *J. Phys. Chem. B* **2006**, *110*, 19586–19592.
(34) Grabuleda, X.; Jaime, C.; Kollman, P. *J. Comput. Chem.* **2000**, *21*, 901–908.
(35) Gaussian 03, Revision C.02, Frisch, M. J.; Trucks, G. W.; Schlegel, H. B.; Scuseria, G. E.; Robb, M. A.; Cheeseman, J. R.; Montgomery, J. A., Jr.; Vreven, T.; Kudin, K. N.; Burant, J. C.; Millam, J. M.; Iyengar, S. S.; Tomasi, J.; Barone, V.; Mennucci, B.; Cossi, M.; Scalmani, G.; Rega, N.; Petersson, G. A.; Nakatsuji, H.; Hada, M.; Ehara, M.; Toyota, K.; Fukuda, R.; Hasegawa, J.; Ishida, M.; Nakajima, T.; Honda, Y.; Kitao, O.; Nakai, H.; Klene, M.; Li, X.; Knox, J. E.; Hratchian, H. P.; Cross, J. B.; Bakken, V.; Adamo, C.; Jaramillo, J.; Gomperts, R.; Stratmann, R. E.; Yazyev, O.; Austin, A. J.; Cammi, R.; Pomelli, C.; Ochterski, J. W.; Ayala, P. Y.; Morokuma, K.; Voth, G. A.; Salvador, P.; Dannenberg, J. J.; Zakrzewski, V. G.; Dapprich, S.; Daniels, A. D.; Strain, M. C.; Farkas, O.; Farkas, O.; Malick, D. K.; Rabuck, A. D.; Raghavachari, K.; Foresman, J. B.; Ortiz, J. V.; Cui, Q.; Baboul, A. G.; Clifford, S.; Cioslowski, J.; Stefanov, B. B.; Liu, G.; Liashenko, A.; Piskorz, P.; Komaromi, I.; Martin, R. L.; Fox, D. J.; Keith, T.; Al-Laham, M. A.; Peng, C. Y.; Nanayakkara, A.; Challacombe, M.; Gill, P. M. W.; Johnson, B.; Chen, W.; Wong, M. W.; Gonzalez, C.; Pople, J. A.; Gaussian, Inc., Wallingford, CT, 2004.
(36) Karpiuk, J.; Svartsov, Y.; Nowacki, J. *Phys. Chem. Chem. Phys.* **2005**, *7*, 4070–4081.
(37) Warshel, A. *Computer Modeling of Chemical Reactions in Enzymes and Solutions*; John Wiley and Sons: NewYork, 1991.
(38) Billeter, S. R.; Webb, S. P.; Iordanov, T.; Agarwal, P. K.; Hammes-Schiffer, S. *J. Chem. Phys.* **2001**, *114*, 6925.
(39) Hu, Z.; Margulis, C. *J. Phys. Chem. B* **2006**, *110*, 11025–11028.
(40) Warshel, A. *J. Phys. Chem.* **1982**, *86*, 2218–2224.
(41) King, G.; Warshel, A. *J. Chem. Phys.* **1990**, *93*, 8682–8692.
(42) Tachiya, M. *J. Phys. Chem.* **1989**, *93*, 7050–7052.
(43) Hwang, J.; Warshel, A. *J. Am. Chem. Soc.* **1987**, *109*, 715–720.
(44) Tachiya, M. *J. Phys. Chem.* **1993**, *97*, 5911–5916.

JP905144N